

# Comprehensive abundance analysis of red giants in the open clusters NGC 2527, 2682, 2482, 2539, 2335, 2251 and 2266

Arumalla B.S. Reddy<sup>1\*</sup>, Sunetra Giridhar<sup>1</sup> and David L. Lambert<sup>2</sup>

<sup>1</sup>*Indian Institute of Astrophysics, Bangalore 560034, India*

<sup>2</sup>*W.J. McDonald Observatory, The University of Texas at Austin, Austin, TX 78712 - 0259, USA*

4 November 2018

## ABSTRACT

We have analyzed high-resolution echelle spectra of red giant members for seven open clusters in the Galactic anticentre direction to explore their chemical compositions. Cluster membership has been confirmed by radial velocity. The spread in temperatures and gravities being very small among the red giants, nearly the same stellar lines were employed for all stars thereby reducing the abundance errors: the errors of the average abundance for a cluster were generally in the 0.02 to 0.05 dex range. Our present sample covers Galactocentric distances of 8.3 to 11.3 kpc and an age range of 0.2 to 4.3 Gyr. A careful comparison of our results for the cluster NGC 2682 (M 67) to other high-resolution abundance studies in the literature shows general good agreement for almost all elements in common.

**Key words:** – Galaxy: abundances – Galaxy: open clusters and associations – stars: abundances: general – open clusters: individual: NGC 2251, NGC 2266, NGC 2335, NGC 2482, NGC 2527, NGC 2539 and NGC 2682

## 1 INTRODUCTION

This is our second paper reporting abundance measurements for red giants in open clusters (OCs) lacking detailed information on their chemical composition. In our first paper (Reddy et al. 2012, hereafter paper 1) we have presented abundance measurements for four open clusters (OCs) whose Galactocentric distances ( $R_{gc}$ ) lie between 8.3 and 10.5 kpc, where the Sun’s Galactocentric distance is taken as  $8.0 \pm 0.6$  kpc (Ghez et al. 2008). Here, we add seven OCs six of which have not previously analysed in detail also in the Galactic anticentre direction in the disc. Our overall goal is to improve understanding of Galactic chemical evolution.

The abundance variation of chemical elements with Galactocentric distance ( $R_{gc}$ ) (i.e., the radial metallicity gradient) along (and across) the disc and the gradient’s temporal variation over the disc’s lifetime put constraints on Galactic chemical evolution models which are controlled, in large part, by variations of such quantities as the initial mass function (IMF), the star formation rate (SFR), gas flows in and out of the disc as well as through the disc. Particularly

informative diagnostics are the spatial and temporal variations of relative abundances which are traditionally referenced to the iron abundance, i.e., ratios such as O/Fe which primarily samples the relative rates of Type II and Type Ia supernovae and Ba/Fe where Ba measures heavy element synthesis by AGB stars.

Abundance variations across the Galaxy, particularly measurements of the radial gradient, have been measured using a wide variety of objects including H II regions, hot young stars, Cepheid variables, planetary nebulae, red giants, and OCs. Various disagreements and inconsistencies remain - see, for example, Magrini et al. (2010). OCs either through spectroscopy of their red giants or cooler main sequence stars provide not only abundance estimates for many elements – essentially, elements sampling all the major processes of stellar nucleosynthesis – but a collection of stars with a well determined age, distance and metallicity. Moreover, it is possible to estimate from an OC’s space motion and a model of the Galactic gravitational potential the birthplace of the OC.

OCs dissolve over time thanks to tidal forces and feed stars into the field. Intracluster abundance variations, especially in the  $\alpha$ - and the heavy elements provide, in principle, a way to chemically tag groups of field stars to their parent cluster (Freeman & Bland-Hawthorn, 2002; De Silva et al.

\* E-mail: sudha@iiap.res.in (ABSR); giridhar@iiap.res.in (SG); dll@astro.as.utexas.edu (DLL)

2006, 2007). Such studies benefit from the largest possible sample of OCs with all properties analysed homogeneously with high-resolution spectroscopy.

Addressing abundance variations across the Galactic disk and applying chemical tagging requires homogeneous and accurate abundance analyses of as large a sample of OCs as possible. In this paper, we continue our modest efforts in this regard by extending our homogeneous abundance analysis for a sample of seven OCs for many elements including the s- and r-process elements for which the measurements are often lacking in the literature.

The layout of the present paper is as follows: In Section 2 we describe the data selection, observations and data reduction, and Section 3 is devoted to the abundance analysis. In Section 4 we present our results and compare them with the abundances derived from samples of field giants. Finally, in Section 5 we give the conclusions.

## 2 OBSERVATIONS AND DATA REDUCTION

Red giant members of OCs, with the exception of NGC 2682 (M67), not yet subjected to a comprehensive abundance analysis using high resolution spectroscopy were selected from the *New catalogue of optically visible open clusters and candidates*<sup>1</sup> (Dias et al. 2002). Selection of red giants instead of main sequence stars enables the extension of our observations to more distant OCs. We have made use of the WEBDA<sup>2</sup> database for the selection of suitable red giant candidates.

Target clusters and their properties are shown in the Table 1: column 1 represents the cluster name, columns 2 & 3 the Galactic longitude and latitude in degrees, column 4 the age, column 5 the photometric estimate of the iron abundance, column 6 the Galactocentric distance, column 7 the distance modulus, column 8 the reddening, column 9 the reference to the photometric [Fe/H]. All quantities are from the database entry except for the photometric [Fe/H] abundance and the Galactocentric distance,  $R_{gc}$ , which we calculate assuming a distance of the Sun from the Galactic centre of  $8.0 \pm 0.6$  kpc (Ghez et al. 2008).

High-resolution optical spectra of the program stars were obtained during the nights of 2011 January 12-14 and March 15-18 with the Robert G. Tull echelle coude spectrograph (Tull et al. 1995) on the 2.7-m Harlan J. Smith telescope at the McDonald observatory using a 2048 x 2048 pixel Tektronix charge-coupled device (CCD) as a detector. The spectra correspond to a resolving power of  $\gtrsim 55,000$  ( $< 6 \text{ km s}^{-1}$ ) as measured by the FWHM of Th I lines in comparison spectra. The spectral coverage in a single exposure from 4000 Å to 5600 Å across various orders was complete but incomplete from 5600 Å to about 9800 Å, where the inter-order gaps begin to appear. In order to minimize the effect of cosmic rays and to acquire a good signal-to-noise (S/N) ratio for our spectra, two or three exposures were taken each lasting for 20-30 min depending on the magnitude of the star.

The basic observation procedure and the data reduction

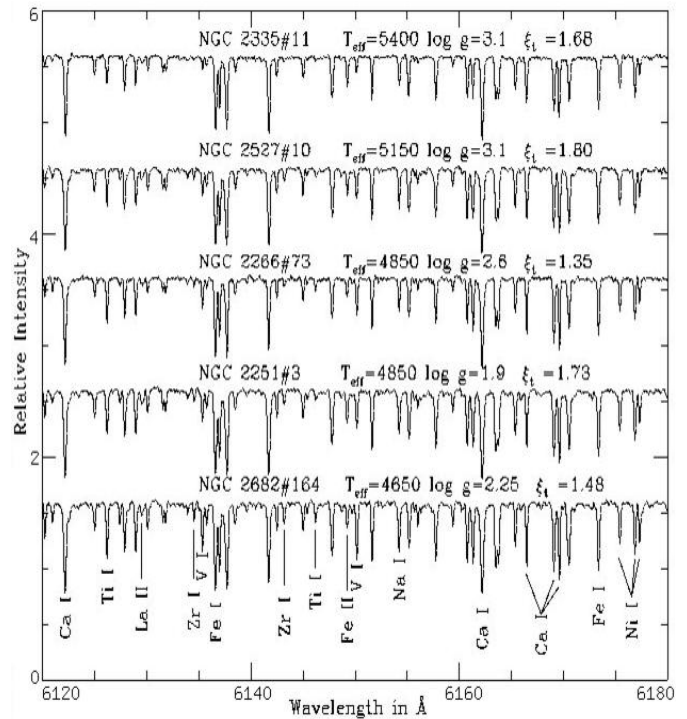


**Figure 1.** Representative spectra of the red giant members of the five open clusters described in Table 1

techniques are same as those listed in our paper I. The echelle spectroscopic data is extracted to one-dimensional spectra with y-axis as flux and the x-axis as wavelength, using the standard spectral reduction software IRAF<sup>3</sup>.

Multiple exposure frames from each of the stars were median combined to acquire optimal S/N ratio and then trimmed to reduce the edge effects during the continuum fitting. The final extracted spectra have S/N ratio of about 100–190 as measured around 6000 Å region, while at wavelengths shorter than 5000 Å the S/N ratio decreases with decreasing wavelength. The continuum fitting was done interactively by marking continuum regions on an each aperture which were then fitted by a cubic spline of appropriate order for proper continuum fitting.

We measured the radial velocity (RV) of each star from its continuum-fitted spectrum using the cores of weak and moderately strong lines of various atomic species. Observed radial velocities were converted to heliocentric velocities using the *rvcorrect* routine available in IRAF software. Our radial velocity measurements are in good agreement with the previous radial velocity measurements for the red giants in OCs (Mermilliod et al. 2008). But, for NGC 2266, no radial velocity measurements from high-resolution spectra are available in the literature. Recently, Carrera (2012) analyzed medium-resolution spectra ( $R \sim 8000$ ) in the infrared CaT region ( $\sim 8500$  Å) for stars in NGC 2266 and derived a mean radial velocity of  $\langle RV \rangle = -16 \pm 15 \text{ km s}^{-1}$

<sup>3</sup> IRAF is a general purpose software system for the reduction and analysis of astronomical data distributed by NOAO, which is operated by the Association of Universities for Research in Astronomy, Inc. under cooperative agreement with the National Science Foundation.

<sup>1</sup> <http://www.astro.iag.usp.br/wilton/>

<sup>2</sup> <http://www.univie.ac.at/webda/>

**Table 1.** Target clusters and their properties from the literature.

Cluster	$\ell$ (deg.)	b (deg.)	Age (Gyr)	[Fe/H] <sub>phot.</sub> (dex.)	R <sub>gc</sub> (kpc)	(m-M) <sub>V</sub> (mag.)	E(B-V) (mag.)	[Fe/H] <sub>ref</sub>
NGC 2251	203.58	+00.10	0.27	-0.20	9.2	11.19	0.19	Parisi et al. (2005)
NGC 2266	187.79	+10.29	1.20	-0.39	11.3	12.97	0.10	Kaluzny et al. (1991)
NGC 2335	223.60	-01.18	0.16	-0.03	9.1	11.98	0.39	Twarog et al. (1997)
NGC 2482	241.62	+02.03	0.40	+0.12	8.7	10.93	0.09	Twarog et al. (1997)
NGC 2527	246.08	+01.85	0.45	-0.09	8.3	09.01	0.04	Piatti et al. (1995)
NGC 2539	233.70	+11.11	0.37	-0.20	8.9	10.93	0.08	Claria & Lapasset (1986)
NGC 2682	215.69	+31.89	4.30	0.00	8.6	9.97	0.06	Dinescu et al. (1995)

**Table 2.** The observed stars

Cluster	Star ID	$\alpha$ (2000.0) (hh mm s)	$\delta$ (2000.0) ( $^{\circ}$ " ')	V (mag.)	B-V (mag.)	V-K <sub>s</sub> (mag.)	J-K <sub>s</sub> (mag.)	$RV_{\text{helio}}$ (km s <sup>-1</sup> )	S/N at 6000 Å
NGC 2251	3	06:34:51.24	+08:19:31.90	10.39	+1.22	+2.92	+0.72	+26.2±0.2	150
	33	06:34:37.07	+08:21:39.50	10.39	+1.21	+2.91	+0.70	+26.3±0.2	150
NGC 2266	73	06:43:16.69	+26:57:05.19	11.06	+0.99	+2.46	+0.69	-29.7±0.2	100
NGC 2335	11	07:06:11.42	-09:56:22.70	10.89	+1.13	+2.76	+0.67	-3.21±0.1	160
NGC 2482	9	07:55:09.09	-24:22:30.25	10.27	+1.11	+2.38	+0.61	+39.00±0.2	190
NGC 2527	10	08:04:46.97	-28:07:50.04	09.49	+0.95	+2.17	+0.59	+40.7±0.2	170
	203	08:05:33.91	-28:08:58.44	09.51	+0.98	+2.21	+0.59	+40.4±0.2	180
NGC 2539	346	08:10:23.02	-12:50:43.25	10.92	+0.99	+2.28	+0.57	+29.7±0.2	130
	463	08:10:42.87	-12:40:11.80	10.69	+1.03	+2.42	+0.60	+28.7±0.2	135
NGC 2682	84	08:51:12.73	+11:52:42.68	10.51	+1.11	+2.53	+0.67	+35.2±0.2	130
	151	08:51:26.22	+11:53:52.23	10.48	+1.10	+2.52	+0.66	+35.0±0.2	120
	164	08:51:29.03	+11:50:33.40	10.52	+1.11	+2.56	+0.61	+34.3±0.1	120

based on four stars. For this cluster, we selected the star with ID 73 whose membership has been confirmed through photometry (Kaluzny & Mazur 1991). Our radial velocity estimate for this OC would appear to be the first measurement available in the literature with negligible dispersion whereas Carrera’s measurement suffers from large uncertainty around the mean. Our radial velocity measurement for this OC differs from the Carrera’s value by  $-10 \text{ km s}^{-1}$ , but is well within the quoted uncertainty in Carrera (2012).

The identification and basic observational data for the stars observed in each of the clusters are given in Table 2 along with the (V-K<sub>s</sub>) and (J-K<sub>s</sub>) colors from the Two Micron All Sky Survey (2MASS) catalogue<sup>4</sup> (Cutri et al. 2003)<sup>5</sup>, computed radial velocity and S/N of each of the spectra extracted at 6000 Å for each of the stars. Spectra of a representative region are shown in Figure 1 for one star from a sample of the five OCs.

### 3 ABUNDANCE ANALYSIS

#### 3.1 Line selection

Our selection criteria for suitable stellar features from each spectra followed the precepts discussed in paper I. The equivalent widths (EWs) for each of the selected absorption features were measured manually using the routine *splot*

contained in IRAF by fitting often a Gaussian profile. But for lines with significant damping wings a Voigt profile was used, for a few lines a direct integration was preferred as a best measure of EW. The final linelist includes 250 lines of 23 elements covering the spectral range 4500 ~ 8850 Å. Our selection criteria provides, on average across the sample of 12 stars, a list of 60 Fe I lines with lower excitation potentials (LEPs) ranging from 0.9 to 5.0 eV, and 12 Fe II lines with LEPs of 2.8 to 3.9 eV and EWs up to 120 mÅ. The line list is essentially that given in Table 3 of Paper I.

Several lines may be affected by telluric absorption lines. The EWs for these lines have been measured only when they appear to be Doppler shifted away from the telluric components, as judged by referring to the Arcturus spectrum (Hinkle et al. 2000).

#### 3.2 Determination of atmospheric parameters

##### 3.2.1 Photometry

The initial determination of effective temperature for each red giant was derived from dereddened<sup>6</sup> B, V, J and K photometry using the empirically calibrated color-temperature relations by Alonso et al. (1999). The corresponding errors around the (B-V), (V-K) and (J-K) relations are 167 K, 25

<sup>4</sup> <http://irsa.ipac.caltech.edu/applications/Gator>

<sup>5</sup> Originally published in University of Massachusetts and Infrared Processing and Analysis Center (IPAC)/ California Institute of Technology.

<sup>6</sup> The adopted interstellar extinctions are  $(A_V, A_K, E(V-K), E(J-K)) = (3.1, 0.28, 2.75, 0.54) * E(B-V)$ , where  $E(B-V)$  is taken from WEBDA

K and 125 K. Before that the 2MASS  $K_s$ <sup>7</sup> magnitudes are transformed to standard K magnitude using the relations given in Carpenter (2001). The mean difference between the two magnitudes is  $K_s = K + (-0.044 \pm 0.003)$ .

The surface gravities were computed by incorporating the known distance to the OCs, effective temperature  $T_{\text{eff},*}$ , bolometric correction  $BC_V$ , and the cluster turn-off mass  $M_*$  into the relation given by (Allende Prieto et al. 1999).  $\log g_* = \log g_\odot + \log(M_*/M_\odot) + 4 \log(T_{\text{eff},*}/T_{\text{eff},\odot})$

$$+ 0.4(V_0 + BC_V) + 2 \log \pi + 0.12 \quad (1)$$

with the corresponding luminosity given by

$$\log(L_*/L_\odot) = -[0.4(V_0 + BC_V) + 2 \log \pi + 0.12] \quad (2)$$

where  $\pi$  is the parallax and  $V_0$  is the dereddened Johnson V magnitude and the bolometric correction  $BC_V$  are derived from estimated effective temperatures and metallicity  $[\text{Fe}/\text{H}]_{\text{phot}}$  in Table 1 from the calibration by Alonso et al. (1999). We adopt  $\log g_\odot = 4.44 \text{ cm s}^{-2}$  and  $T_{\text{eff},\odot} = 5777 \text{ K}$ .

A cluster's turn-off mass has been estimated from the stellar evolutionary tracks by Yi et al. (2003): turn-off masses are  $3.3 M_\odot$  for NGC 2251,  $2.1 M_\odot$  for NGC 2266,  $3.8 M_\odot$  for NGC 2335,  $3.0 M_\odot$  for NGC 2482,  $2.8 M_\odot$  for NGC 2527,  $3.1 M_\odot$  for NGC 2539 and  $1.4 M_\odot$  for NGC 2682. Red giants are assumed to have the turn-off mass in computing the surface gravity.

Assuming that the various quantities involved in equations (1) & (2) are independent of each other and by introducing an error of 10% in the stellar mass, an uncertainty of 3% in  $T_{\text{eff},*}$ , an uncertainty of 5% in photometric V magnitude and the bolometric corrections, and an error of 10% in the distance (i.e., the parallax), we estimate an error of  $\simeq 0.11$  dex in  $\log g_*$  with an uncertainty of 0.08 in  $\log L_*$ .

### 3.2.2 Spectroscopy

The spectroscopic abundance analysis was executed using the latest version (2010) of the local thermodynamical equilibrium (LTE) line analysis and spectrum synthesis code **MOOG** developed by Chris Sneden and originally described in Sneden (1973)<sup>8</sup>. Model atmospheres were interpolated linearly from the ATLAS9 model atmosphere grid of Castelli & Kurucz (2003)<sup>9</sup>. For this purpose, initially we used a model with photometrically determined atmospheric parameters. These models assume a line-blanketed plane-parallel uniform atmospheres in LTE and hydrostatic equilibrium with flux conservation.

The linelist (Table 13 available online) and basic atomic line data (see Table 3 of paper I) give reference solar abundances that agree well with the published values from Asplund et al. (2009). We performed a differential abundance analysis relative to the Sun by running the **MOOG** in *abfind* mode using the initially estimated stellar parameters (see., Section 3.2.1) and the measured EWs. This *abfind* driver

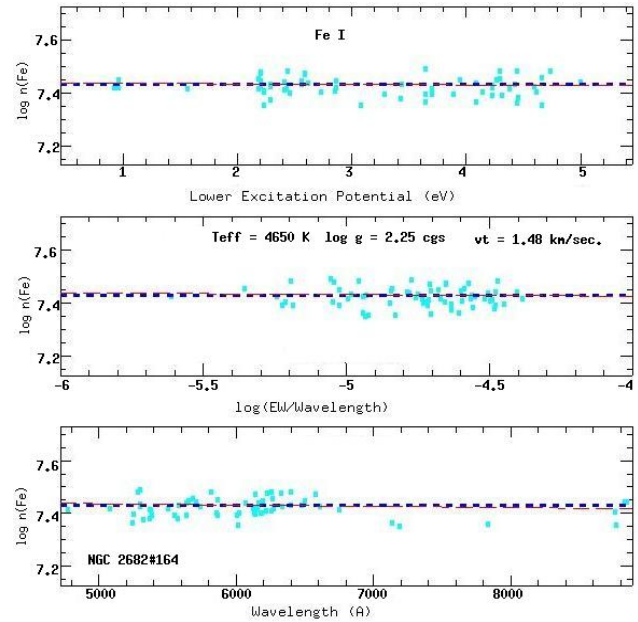


**Figure 2.** The observed trends for the derived abundance from the Fe I lines,  $[\text{Fe I}/\text{H}]$ , for the star NGC 2682#164 as a function of LEP (upper panel), reduced equivalent width (lower panel), and the wavelength of each line (lower panel).

force-fits the individual line abundances to match the computed EWs to the observed ones, previously measured using the *splot* routine of IRAF.

First, we estimated the microturbulence velocity,  $\xi_t$ , using Fe II lines instead of Fe I, since Fe II lines are less affected by the departures from LTE. The  $\xi_t$  is determined by the requirement that the abundance from Fe II line generally chosen to have small range in LEP (2.8-3.9 eV) but a good range in their EWs, are independent of line's EW or reduced EW ( $\log(\text{EW}/\lambda)$ ). The  $T_{\text{eff}}$  is estimated by the requirement that the Fe abundance from Fe I lines is independent of a line's LEP. Finally, the surface gravity,  $\log g$ , is estimated from the constraint that Fe I and Fe II lines give the same Fe abundance for the derived  $T_{\text{eff}}$  and  $\xi_t$ .

In Figure 2, we show a graphical representation of the determination of atmospheric parameters using Fe I line abundances as a function of line's LEP, line strength, and the wavelength of the lines for a typical star (NGC 2682#164) together with a linear fit to each distribution. The vertical axis gives the logarithmic iron abundance on the standard scale in which  $\log \epsilon(\text{H}) = 12$ . The thick dashed blue lines represent the mean Fe I abundance, and the thin dashed red lines represent linear trends of abundance with the three variables. The lack of significant trends of the iron abundance with LEP (upper panel) and line strength (middle panel) supports the validity of our chosen model and the adopted  $\xi_t$ . The absence of any trend between the derived iron abundance and the wavelength (bottom panel) represents a check on our continuum placement.

A check on the derived spectroscopic atmospheric parameters was performed in the same way as described in paper I. In short, the uncertainty in the microturbulence is estimated from the spread in the derived abundance as computed from Fe I/Fe II, Ti I/Ti II, V I and Cr I/Cr II,

<sup>7</sup> The 2MASS survey uses a K-short ( $K_s$ ) filter whose effective wavelength is centred around 2.16 microns in the near-infrared.

<sup>8</sup> <http://www.as.utexas.edu/chris/moog.html>

<sup>9</sup> <http://kurucz.harvard.edu/grids.html>

**Table 3.** Basic photometric and spectroscopic atmospheric parameters for the stars in each cluster.

Cluster	Star ID	$T_{\text{eff}}^{\text{phot}}$ (K)			$\log g_{\text{phot}}^{(V-K)}$ ( $\text{cm s}^{-2}$ )	$T_{\text{eff}}^{\text{spec}}$ (K)	$\log g_{\text{spec}}$ ( $\text{cm s}^{-2}$ )	$\xi_{\text{spec}}$ ( $\text{km sec}^{-1}$ )	$\log(L/L_{\odot})$ spectroscopy	$\log(L/L_{\odot})$ photometry
		(B-V)	(V-K)	(J-K)						
NGC 2251	3	4620	4642	4575	2.21	4850	1.90	1.73	2.75	2.36
	33	4693	4647	4624	2.24	4850	2.00	1.67	2.65	2.31
NGC 2266	73	4953	4910	4564	1.80	4850	2.60	1.35	1.85	2.67
NGC 2335	11	5372	5509	5145	2.51	5400	3.10	1.68	1.80	2.43
NGC 2482	9	4802	4945	4756	2.34	4850	2.50	1.73	2.10	2.29
NGC 2527	10	4946	4994	4740	2.80	5150	3.10	1.80	1.59	1.84
	203	4884	4950	4734	2.78	5050	2.80	1.61	1.85	1.84
NGC 2539	346	4934	5002	4888	2.63	5175	3.10	1.70	1.64	2.05
	463	4840	4844	4794	2.47	5050	2.80	1.68	1.90	2.15
NGC 2682	84	4702	4683	4508	2.36	4800	2.60	1.55	1.66	1.85
	151	4720	4696	4552	2.36	4700	2.25	1.38	1.98	1.87
	164	4702	4658	4712	2.36	4650	2.25	1.48	1.96	1.85

around its minima while the microturbulence is varied over the range from 0 to 6  $\text{km s}^{-1}$  (See Figure 2 in our paper I for illustration). The uncertainty in the  $\log g$  value is provided by the ionization equilibrium between neutral and ionized species of the elements Sc, Ti, V and Cr. Finally, the uncertainty in the  $T_{\text{eff}}$  is acquired by inspecting the slope of the relation between the Fe I abundance and LEPs of the lines. Therefore, the typical uncertainties estimated in this analysis are 100 K in  $T_{\text{eff}}$ , 0.25  $\text{cm s}^{-2}$  in  $\log g$  and 0.20  $\text{km s}^{-1}$  in  $\xi_t$ .

The derived stellar parameters for program stars in each of the cluster are shown in Table 3: column 1 represents the cluster name, column 2 represents the star ID, columns 3 & 4 represent the photometric  $T_{\text{eff}}$  using (B-V), (V-K) and (J-K) and  $\log g$  values, columns 5-7 represent the spectroscopic  $T_{\text{eff}}$ ,  $\log g$  and  $\xi_t$  estimates. Finally, the spectroscopic and photometric luminosities ( $\log(L/L_{\odot})$ ) are presented in columns 8 & 9. The mean difference in effective temperatures estimated using (B-V) and (V-K) is  $-26 \pm 64$  K and using (V-K) and (J-K) is  $+157 \pm 121$  K. The corresponding mean differences in  $T_{\text{eff}}^{(B-V)}$ ,  $T_{\text{eff}}^{(V-K)}$  and  $T_{\text{eff}}^{(J-K)}$  with respect to spectroscopic  $T_{\text{eff}}^{\text{spec}}$ s are  $-100 \pm 113$ K,  $-75 \pm 116$ K and  $-232 \pm 117$ K respectively. Mean differences in  $\log g$  and  $\log(L/L_{\odot})$  across the 12 stars are  $-0.18 \pm 0.33$   $\text{cm-s}^{-2}$  and  $-0.15 \pm 0.35$   $\text{cm-s}^{-2}$  respectively.

The photometric  $T_{\text{eff}}$ 's derived from the calibrations based on infrared flux method (Alonso et al. 1999) are sensitive to the adopted colors, reddening estimates and metallicity. When using the (B-V)–  $T_{\text{eff}}$  calibration an error of 0.03 mag on (B-V) and a conservative uncertainty of 20 % in reddening translates into a temperature uncertainty of 1.1 to 1.3 % each. Equivalently, an error of 0.2 dex in  $[\text{Fe}/\text{H}]_{\text{phot}}$  implies a temperature uncertainty of 1.2 %. When using the (V-K)–  $T_{\text{eff}}$  calibration, we note that an error of 0.03 mag on (V-K) and an uncertainty of 20 % in reddening implies a temperature uncertainty of 0.1 to 0.7 % each and an error of 0.2 dex in  $[\text{Fe}/\text{H}]_{\text{phot}}$  implies a temperature uncertainty of 0.1 to 0.9 %. Even though the  $T_{\text{eff}}$  as a function of (J-K) has no dependence on metallicity, an error of 0.03 mag on (J-K) implies a temperature uncertainty of 2 % while the effect of reddening variation is less. As we have shown in Paper I, temperatures derived from (V-K) colour might be least affected by photometric uncertainties and we shall use

these values as the photometric  $T_{\text{eff}}$  estimates of our giant stars.

With few exceptions, our spectroscopic estimates are in good agreement with the photometric ones. The uncertainty affecting latter is subject to the uncertainties in the reddening values. For example, for NGC 2251 the difference in  $T_{\text{eff}}^{(V-K)}$  and  $T_{\text{eff}}^{\text{spec}}$  is around 200 K using the reddening estimate of  $E(B-V) = 0.186$  as quoted in WEBDA database. If we replace this value with the one ( $E(B-V) = 0.21 \pm 0.03$ ) given in the recent analysis of Parisi et al. (2005), the difference between the two temperatures will be reduced by 50-100 K. The corresponding comparison of the spectroscopic  $[\text{Fe}/\text{H}]$  with the photometric one in Table 1 also illustrates fair agreement:  $\Delta[\text{Fe}/\text{H}] = 0.10$  (NGC 2251),  $-0.05$  (NGC 2266),  $-0.15$  (NGC 2335),  $-0.19$  (NGC 2482),  $-0.01$  (NGC 2527), 0.14 (NGC 2539) and  $-0.08$  (NGC 2682).

### 3.3 Abundances and error estimation

Once the atmospheric parameters were estimated from the spectral line measurements as described in previous section, the corresponding model atmospheres were used in *abfind* and *synth* drives of MOOG to conduct a complete abundance analysis. In most cases, the abundances are derived from the measured EWs but a few lines were analysed with synthetic spectra.

Synthetic spectra were computed for species affected by hyperfine and isotopic splitting or affected by blends. Lines treated by synthesis included: Sc II (6245 Å), Mn I (6013 Å and 6021 Å), V I (5727 Å), Cu I (5218 Å), Rb I (7800 Å), Ba II (5853 Å) and Eu II (6645 Å) by including their hfs components, and Ce II (5472 Å) and Sm II (4577 Å). We adopted the hfs data and isotopic ratios listed in Paper I. The hfs data and isotopic ratios for the Eu II line has been kindly provided by C. Sneden whose linelist uses the  $gf$ -values provided by Lawler et al. (2001). For the Rb I line, the number of hfs components, the accurately known wavelengths and the relative strength of each component were taken from Lambert & Luck's (1976) analysis of the Rb I resonance line in the Arcturus spectrum and a reliable  $\log gf$  value of  $+0.13 \pm 0.04$  from Wiese & Martin (1980). A fit to this line includes a Si I blend to the blue. As there are no reliable measurements of experimental  $gf$ -values for this line, we have adopted a solar  $gf$ -value of  $-0.75$  to model the

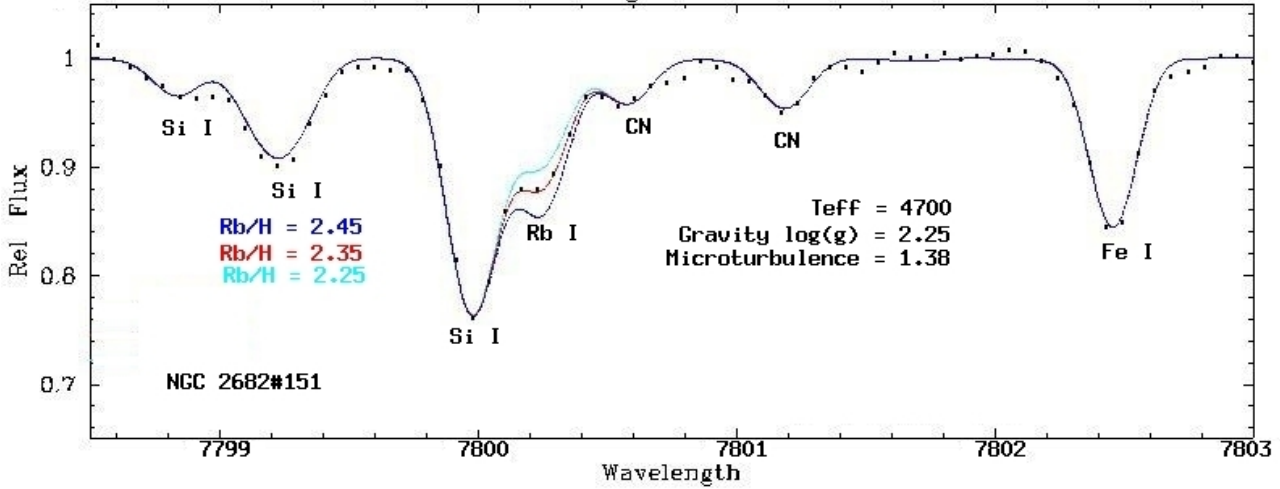


**Figure 3.** Synthetic spectra (continuous lines) and the observed spectrum (dotted line) of NGC 2682 #151 around the Rb I line at 7800 Å. The indicated abundances in the figure are on a logarithmic scale.

solar Si I line profile from the solar integrated disc spectrum (Kurucz et al. 1984). Our solar abundance measurement of  $\log \epsilon_{\odot} = 2.60$  dex for the Rb is in close agreement with Asplund et al's. (2009) value of  $\log \epsilon_{\odot} = 2.52 \pm 0.10$  dex.

A fit to the Rb I line at 7800 Å in the observed spectrum (dotted line) of NGC 2682 #151 is shown in figure 3 as solid lines with  $[\text{Rb}/\text{H}] = 2.35 \pm 0.10$  dex, based on  $\chi^2$  goodness of fit provided by MOOG. A visual inspection of the figure shows that the red line ( $[\text{Rb}/\text{H}] = 2.35$ ) is a better match to the stellar spectrum.

The largest hfs correction is about  $-0.11$  dex for  $[\text{Sc}/\text{Fe}]$ ,  $-0.10$  dex for  $[\text{V}/\text{Fe}]$ ,  $-0.43$  dex for  $[\text{Mn}/\text{Fe}]$ ,  $-0.39$  dex for  $[\text{Cu}/\text{Fe}]$ ,  $-0.12$  dex for  $[\text{Ba}/\text{Fe}]$ ,  $-0.32$  dex for  $[\text{Eu}/\text{Fe}]$ .

Abundance results for the individual stars in each of the OCs are presented in Tables 8–12. For each abundance based on the analysis of EWs, the abundance and standard deviation were calculated from all lines of given species. The tables give the  $[\text{Fe}/\text{H}]$  and  $[\text{X}/\text{Fe}]$  for elements considered here relative to solar abundances derived from the adopted  $gf$ -values. Therefore, errors in the adopted  $gf$  values are unimportant when providing differential abundances ( $[\text{X}/\text{H}]$  or  $[\text{X}/\text{Fe}]$ ) provided that the solar and stellar abundances depend on the same set of lines.

Inspection of the Tables 8–12 shows that, in general, the compositions  $[\text{X}/\text{Fe}]$  of stars in a given cluster are generally identical to within the (similar) standard deviations computed for an individual star. Exceptions tend to occur for species represented by one or a few lines, as expected when the uncertainty in measuring equivalent widths is a contributor to the total uncertainty. From the spread in the abundances for the stars of a given cluster we obtain the standard deviation  $\sigma_1$  in the Tables 8–11 in the column headed ‘average’.

We evaluated the sensitivity of the derived abundances to the uncertainties in the adopted atmospheric parameters by varying each time only one of the parameters by the amount corresponding to the typical error. The changes in abundances caused by varying atmospheric parameters by 100 K,  $0.25 \text{ cm s}^{-2}$  and  $0.2 \text{ km s}^{-1}$  with respect to the chosen model atmosphere are summarized in Table 4. We

**Table 4.** Sensitivity of abundances to the uncertainties in the model parameters for the star with ID 11 in NGC 2335 with  $T_{\text{eff}} = 5400 \text{ K}$ ,  $\log g = 3.10 \text{ cm s}^{-2}$ , and  $\xi_t = 1.68 \text{ km s}^{-1}$ .

Species	$T_{\text{eff}} \pm 100 \text{ K}$	$\log g \pm 0.25$	$\xi_t \pm 0.20$	$\sigma_2$
	$\sigma_{T_{\text{eff}}}$	$\sigma_{\log g}$	$\sigma_{\xi_t}$	
Na I	+0.05/−0.06	−0.02/+0.02	−0.04/+0.05	0.04
Mg I	+0.03/−0.03	−0.01/+0.01	−0.02/+0.03	0.02
Al I	+0.03/−0.04	−0.01/+0.01	−0.02/+0.02	0.02
Si I	+0.01/−0.01	+0.03/−0.02	−0.02/+0.02	0.02
Ca I	+0.07/−0.08	−0.02/+0.02	−0.09/+0.09	0.07
Sc I	+0.09/−0.09	0.00/+0.01	0.00/+0.01	0.05
Sc II	−0.02/+0.01	+0.12/−0.11	−0.05/+0.06	0.07
Ti I	+0.10/−0.12	−0.01/0.00	−0.03/+0.03	0.06
Ti II	−0.03/+0.01	+0.11/−0.12	−0.07/+0.08	0.08
V I	+0.12/−0.13	−0.01/0.00	−0.01/+0.01	0.05
Cr I	+0.08/−0.10	−0.01/0.00	−0.07/+0.07	0.06
Cr II	−0.05/+0.04	+0.11/−0.11	−0.05/+0.06	0.07
Mn I	+0.07/−0.09	0.00/−0.01	−0.04/+0.04	0.05
Fe I	+0.08/−0.09	0.00/0.00	−0.09/+0.10	0.07
Fe II	−0.07/+0.05	+0.12/−0.13	−0.07/+0.07	0.09
Co I	+0.08/−0.08	+0.01/−0.01	−0.01/+0.02	0.05
Ni I	+0.07/−0.06	+0.02/−0.02	−0.05/+0.05	0.05
Cu I	+0.07/−0.08	+0.02/−0.02	−0.04/+0.06	0.05
Zn I	+0.02/+0.03	+0.07/−0.06	−0.05/+0.07	0.05
Rb I	+0.07/−0.08	−0.01/0.00	−0.01/0.00	0.04
Y II	−0.01/−0.01	+0.11/−0.12	−0.07/+0.09	0.08
Zr I	+0.13/−0.13	0.00/−0.01	0.00/+0.01	0.07
Zr II	−0.01/0.00	+0.10/−0.11	−0.01/+0.01	0.06
Ba II	+0.01/−0.03	+0.08/−0.10	−0.17/+0.17	0.11
La II	0.00/−0.02	+0.10/−0.12	−0.02/+0.01	0.06
Ce II	−0.01/−0.01	+0.10/−0.11	−0.01/+0.01	0.06
Nd II	+0.01/−0.02	+0.11/−0.11	−0.02/+0.02	0.06
Sm II	+0.02/−0.01	+0.11/−0.11	−0.02/+0.03	0.06
Eu II	−0.01/0.00	+0.11/−0.11	−0.01/+0.01	0.06

quadratically added the three contributors, by taking the square root of the sum of the square of individual errors associated with uncertainties in temperature, gravity and microturbulence, to obtain  $\sigma_2$ . The total error  $\sigma_{\text{tot}}$  for each of the element is the quadratic sum of  $\sigma_1$  and  $\sigma_2$ . The error bars in the abundance tables correspond to this total

**Table 5.** Elemental abundance ratios  $[X/Fe]$  for elements from Na to Eu for a sample seven OCs from this study

Species	NGC 2527	NGC 2682	NGC 2482	NGC 2539	NGC 2335	NGC 2251	NGC 2266
[Na I/Fe]	+0.32 ± 0.03	+0.25 ± 0.03	+0.30 ± 0.03	+0.27 ± 0.03	+0.24 ± 0.03	+0.33 ± 0.04	+0.23 ± 0.03
[Mg I/Fe]	+0.07 ± 0.01	+0.16 ± 0.02	+0.13 ± 0.02	+0.07 ± 0.02	+0.08 ± 0.02	+0.06 ± 0.02	+0.39 ± 0.02
[Al I/Fe]	+0.05 ± 0.02	+0.09 ± 0.01	+0.07 ± 0.02	0.00 ± 0.01	-0.02 ± 0.02	0.00 ± 0.02	+0.25 ± 0.02
[Si I/Fe]	+0.20 ± 0.02	+0.20 ± 0.02	+0.23 ± 0.04	+0.17 ± 0.02	+0.10 ± 0.02	+0.23 ± 0.02	+0.28 ± 0.02
[Ca I/Fe]	+0.12 ± 0.04	+0.04 ± 0.04	+0.01 ± 0.05	+0.04 ± 0.04	+0.09 ± 0.04	+0.09 ± 0.05	+0.17 ± 0.05
[Sc I/Fe]	+0.25 ± 0.04	+0.04 ± 0.04	+0.12 ± 0.05	+0.21 ± 0.04	+0.13 ± 0.04	+0.04 ± 0.04	+0.31 ± 0.05
[Sc II/Fe]	+0.12 ± 0.04	+0.10 ± 0.04	+0.08 ± 0.05	+0.04 ± 0.04	<b>+0.16</b>	<b>+0.02</b>	+0.22 ± 0.05
[Ti I/Fe]	+0.11 ± 0.04	-0.01 ± 0.04	+0.01 ± 0.04	+0.10 ± 0.04	+0.17 ± 0.04	-0.04 ± 0.04	+0.23 ± 0.04
[Ti II/Fe]	+0.08 ± 0.04	+0.01 ± 0.05	-0.03 ± 0.04	+0.08 ± 0.04	+0.12 ± 0.04	-0.04 ± 0.04	+0.30 ± 0.04
[V I/Fe]	+0.21 ± 0.04	+0.09 ± 0.05	+0.10 ± 0.05	+0.16 ± 0.04	+0.13 ± 0.03	-0.05 ± 0.05	+0.20 ± 0.06
[Cr I/Fe]	+0.10 ± 0.03	+0.05 ± 0.03	+0.10 ± 0.04	+0.08 ± 0.04	+0.07 ± 0.03	+0.05 ± 0.04	+0.09 ± 0.03
[Cr II/Fe]	+0.06 ± 0.04	+0.08 ± 0.05	+0.09 ± 0.05	+0.08 ± 0.04	0.00 ± 0.04	+0.04 ± 0.05	+0.02 ± 0.04
[Mn I/Fe]	<b>0.00</b>	<b>-0.08</b>	<b>-0.11</b>	<b>+0.01</b>	<b>-0.01</b>	<b>-0.13</b>	<b>-0.01</b>
[Fe I/H]	-0.11 ± 0.04	-0.08 ± 0.04	-0.07 ± 0.04	-0.06 ± 0.04	-0.19 ± 0.04	-0.10 ± 0.05	-0.45 ± 0.04
[Fe II/H]	-0.09 ± 0.05	-0.08 ± 0.05	-0.07 ± 0.05	-0.07 ± 0.05	-0.17 ± 0.05	-0.10 ± 0.05	-0.43 ± 0.05
[Co I/Fe]	+0.16 ± 0.04	+0.11 ± 0.02	+0.11 ± 0.03	+0.07 ± 0.02	+0.16 ± 0.04	+0.03 ± 0.03	+0.27 ± 0.03
[Ni I/Fe]	+0.06 ± 0.02	+0.10 ± 0.03	+0.03 ± 0.04	+0.02 ± 0.02	+0.09 ± 0.03	+0.04 ± 0.03	+0.09 ± 0.03
[Cu I/Fe]	<b>-0.14</b>	<b>-0.03</b>	<b>-0.21</b>	<b>-0.16</b>	<b>-0.15</b>	<b>-0.22</b>	<b>+0.02</b>
[Zn I/Fe]	<b>-0.16</b>	<b>-0.07</b>	<b>-0.22</b>	<b>-0.22</b>	<b>-0.06</b>	<b>-0.13</b>	<b>0.00</b>
[Rb I/Fe]	<b>+0.07</b>	<b>-0.10</b>	<b>-0.13</b>	<b>+0.04</b>	<b>+0.08</b>	<b>-0.17</b>	<b>+0.14</b>
[Y II/Fe]	+0.16 ± 0.04	+0.03 ± 0.04	+0.15 ± 0.04	+0.17 ± 0.04	+0.12 ± 0.05	+0.07 ± 0.04	+0.05 ± 0.04
[Zr I/Fe]	+0.31 ± 0.05	-0.07 ± 0.05	+0.11 ± 0.05	+0.21 ± 0.04	+0.06 ± 0.04	0.00 ± 0.05	-0.08 ± 0.05
[Zr II/Fe]	+0.18 ± 0.03	-0.07 ± 0.03	+0.10 ± 0.04	+0.26 ± 0.03	+0.01 ± 0.03	+0.06 ± 0.03	...
[Ba II/Fe]	<b>+0.08</b>	<b>-0.16</b>	<b>+0.09</b>	<b>+0.10</b>	<b>+0.25</b>	<b>+0.11</b>	<b>-0.13</b>
[La II/Fe]	+0.26 ± 0.03	0.00 ± 0.03	+0.18 ± 0.03	+0.18 ± 0.03	+0.29 ± 0.03	+0.02 ± 0.04	-0.02 ± 0.04
[Ce II/Fe]	<b>+0.24</b>	<b>-0.02</b>	<b>+0.11</b>	<b>+0.20</b>	<b>+0.29</b>	<b>+0.07</b>	<b>-0.07</b>
[Nd II/Fe]	+0.20 ± 0.03	+0.02 ± 0.04	+0.13 ± 0.04	+0.23 ± 0.04	+0.32 ± 0.03	+0.08 ± 0.04	+0.13 ± 0.04
[Sm II/Fe]	<b>+0.18</b>	<b>-0.03</b>	+0.13 ± 0.04	<b>+0.18</b>	+0.28 ± 0.04	<b>+0.02</b>	<b>+0.11</b>
[Eu II/Fe]	<b>+0.10</b>	<b>+0.08</b>	<b>+0.07</b>	<b>+0.19</b>	<b>+0.07</b>	<b>+0.04</b>	<b>+0.40</b>

**Note:** Abundances calculated by synthesis are presented in bold numbers.

error. The final OC mean abundances from this study are presented in Table 5.

#### 4 RESULTS

The addition of these seven clusters to literature sample also supports the widely held impression that there is an abundance gradient such that the metallicity  $[Fe/H]$  at the solar galactocentric distance decreases outwards (Magrini et al. 2009, Yong et al. 2012) at about  $-0.1$  dex  $kpc^{-1}$  and at the same time our sample has not changed the dispersion of metallicities at a given Rgc.

As in Paper I, we compare our results with those from Luck & Heiter (2007) for a large sample of nearby giants whose analysis was similar to our, i.e., a differential analysis with respect to the Sun. Perhaps, the chief advantage of this comparison is that various systematic effects should cancel which would enter into a comparison involving our giants and field main sequence stars. Two obvious issues are non-LTE effects which are, in general, going to be different for giants and dwarfs and the use of classical atmospheres which simulations of stellar granulation show may in different ways be inadequate representation of real stars.

From Luck & Heiter's Table 4, we calculate mean abundances  $[X/Fe]$  for  $[Fe/H]$  from 0.0 to  $-0.2$ , the metallicity spread of six of our seven clusters. NGC 2266 at  $[Fe/H] = -0.44$  is excluded from the sample in part because it may belong to the thick rather than the thin disc. One can ar-

gue based on the membership probabilities (see for example Reddy et al. 2006 for definitions and recipes) derived using the present day cluster's space motions that this cluster has a high probability to belong to the thick disc (Reddy & Giridhar, in preparation). Inspection of Table 6 shows that the mean  $[X/Fe]$  for the six clusters are within 0.10 dex of Luck & Heiter's results except for Na, Ca, Sc, V, Mn, Cu, and Nd and within 0.15 dex for all but Na, Sc, V, and Nd. (Elements Zn, Rb, and Sm were not considered by Luck & Heiter.) Thus, we conclude that field giants and OCs of near-solar metallicity have very similar, if not identical, compositions. This was the conclusion reached also in Paper I.

We review our conclusions made in our paper I for Mn I. Our  $[Mn/Fe]$  ratios for OC giants matches well with Takeda (2008) sample of field giants, while it is lower by 0.12 dex with respect to the local thin disc field giants of Luck & Heiter (2007). Luck & Heiter's (2007) abundance results for field giants are generally confirmed by Takeda et al. (2008) for other large sample of field giants. Indeed, Luck & Heiter's (2007)  $[Mn/Fe]$  abundance ratios for red giants are 0.1 dex lower than their sample of field dwarfs (Luck & Heiter 2006). Both Luck & Heiter's (2007) and Takeda et al. (2008) have employed similar abundance analysis based on the EW measurement of a large set of lines. Determination of the abundances of the elements using EW measurements of the lines is not always recommended as a good approximation for the features affected by hfs components. Moreover, these lines



**Table 6.** Mean elemental abundance ratios,  $[X/Fe]$ , for Na to Eu for the six OCs from this study and the thin disc mean abundances from Luck & Heiter (2007) in the metallicity of our clusters (0.0 to  $-0.2$  dex). Abundances calculated by synthesis are presented in bold typeface.

Species	OC mean	Thin disc
[Na I/Fe]	$+0.28 \pm 0.04$	$+0.10 \pm 0.06$
[Mg I/Fe]	$+0.09 \pm 0.04$	$+0.08 \pm 0.10$
[Al I/Fe]	$+0.03 \pm 0.04$	$+0.09 \pm 0.05$
[Si I/Fe]	$+0.19 \pm 0.05$	$+0.12 \pm 0.04$
[Ca I/Fe]	$+0.07 \pm 0.04$	$-0.04 \pm 0.05$
[Sc I/Fe]	$+0.13 \pm 0.09$	$-0.08 \pm 0.06$
[Ti I/Fe]	$+0.06 \pm 0.08$	$0.00 \pm 0.03$
[V I/Fe]	$+0.11 \pm 0.09$	$-0.09 \pm 0.07$
[Cr I/Fe]	$+0.07 \pm 0.02$	$+0.01 \pm 0.05$
[Mn I/Fe]	<b><math>-0.05 \pm 0.06</math></b>	$+0.06 \pm 0.07$
[Co I/Fe]	$+0.11 \pm 0.05$	$+0.06 \pm 0.08$
[Ni I/Fe]	$+0.06 \pm 0.03$	$0.00 \pm 0.03$
[Cu I/Fe]	<b><math>-0.15 \pm 0.07</math></b>	$+0.01 \pm 0.13$
[Rb I/Fe]	<b><math>-0.04 \pm 0.11</math></b>	...
[Y II/Fe]	$+0.12 \pm 0.06$	$+0.07 \pm 0.15$
[Zr I/Fe]	$+0.10 \pm 0.14$	...
[Zr II/Fe]	$+0.09 \pm 0.12$	...
[Ba II/Fe]	<b><math>+0.09 \pm 0.15</math></b>	$+0.04 \pm 0.16$
[La II/Fe]	$+0.15 \pm 0.12$	$+0.05 \pm 0.09$
[Ce II/Fe]	<b><math>+0.15 \pm 0.12</math></b>	$+0.05 \pm 0.09$
[Nd II/Fe]	$+0.16 \pm 0.11$	$-0.01 \pm 0.07$
[Sm II/Fe]	$+0.13 \pm 0.11$	...
[Eu II/Fe]	<b><math>+0.09 \pm 0.05</math></b>	$+0.08 \pm 0.06$

are typically strong in red giant branch stars than their main sequence counterparts with similar metallicities.

Since, the hfs effect desaturates strong absorption lines and results in features with larger equivalent widths the computed abundances will be overestimated. It will be more complicated for the elements having isotopes due to the superposition of the spectra of the various isotopes of the same element. The relative strength and isotopic shift vary from element to element. Since, the stellar surface abundance estimates are highly dependent on the line strength, it is important to treat strong lines for hfs effects since the hfs correction increases with line strength. For weak lines, those generally lay on the linear part of the curve of growth, the hfs treatment is not so important because they are already unsaturated. Hence a spectrum synthesis over the separate hfs components is recommended to derive an abundance for the lines affected by hfs components. Thus, the number of components, the wavelength splittings, isotopic shifts, if any present, and the relative strength of each component must be known.

In our analysis largest hfs corrections are applied to  $[Mn/Fe]$  ( $\simeq -0.43$  dex). From the Figure 15 of Takeda (2007) for a sample field dwarfs, it is evident that the Mn I lines employed for their abundance analysis are all weak ( $EW < 50$  mÅ) for which they have noted a negligible hfs corrections ( $\simeq -0.02$  dex). Similarly, in their giant sample Takeda et al. (2008) have employed a single weak line at 5004.8 Å for the abundance analysis for which the hfs effects are less important. Whereas the Mn I abundances from Luck & Heiter (2007), similar to ours, might be based on strong lines for which they have not employed hfs treatment, unlike ours.

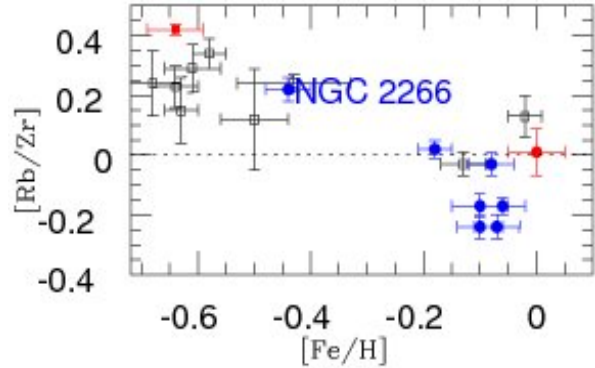


**Figure 4.** The abundance ratio for  $[Rb/Zr]$  as a function of  $[Fe/H]$  with corresponding error bars. The dots (blue) represent the mean cluster abundances derived in this study. The OC NGC 2266 with a largest  $[Rb/Zr]$  ratio ( $= +0.22$ ) is marked in the figure. The empty squares (black) represents the data taken from Tomkin & Lambert (1999) for a sample of metal-deficient disc and halo stars. The filled square and the filled circle (in red) represents the  $[Rb/Zr]$  ratios for Arcturus and Sun. The dotted line indicate the solar mix of elements.

This can fairly explain the observed offset in the abundance trends of field dwarfs and our OCs red giants with the abundance trend of field giants from Luck & Heiter (2007).

The Rb abundance provides an additional diagnostic information on the neutron density at the s-process site which is controlled by both the neutron source and the mass of the parent AGB star responsible for its synthesis. The abundance of Rb relative to its neighboring s-process elements such as Sr, Y and Zr is a useful monitor of neutron density at the time of s-processing. Thanks to the branch in the s-process path at  $^{85}Kr$  with a  $\beta$ -decay half life of 10.7 yr, which at low neutron densities ( $N_n \leq 10^7$  cm $^{-3}$ ) decays to  $^{85}Rb$ , while at higher neutron densities suffers successive neutron captures and the flow proceeds along the path from  $^{85}Kr$  to  $^{86}Kr$  to  $^{87}Kr$ , that  $\beta$ -decays to stable  $^{87}Rb$  isotope. The sensitivity of the Rb elemental abundance to the neutron density arises then due to the quite different neutron capture cross sections for both of its stable isotopes ( $^{85}Rb$  and  $^{87}Rb$ ) among which the  $^{85}Rb$  being roughly a factor 10 times more efficient than  $^{87}Rb$ . Thus, at low neutron densities the ratio  $[Rb/Zr]$  is about 10 times less than that at high neutron densities. Since, the solar Rb abundance is attributed in almost equal parts to the s-process and r-process, the observed stellar Rb abundance directly indicate the neutron density at the s-process site. Even though the stellar Rb I isotopic ratios can not be measured, the Rb I lines used in our analysis are weak in all the program stars so the derived Rb abundances are not affected by changes in the isotopic mixture. We derived the Zr abundances using 5-7 weak lines (see the Tables 8–12 for the number of lines used for each star) for which reliable estimates of  $gf$ -values are available and the usage of the same lines will remove the systematic uncertainties.

A comparison of our observed  $[Rb/Zr]$  abundance ratios for these OCs (Figure 4) with the recent models of AGB nucleosynthesis from Figure 14 in Smith et al. (2000) suggests that the 3  $M_{\odot}$  models provide complete overlap with observations except for the  $[Rb/Zr]$  ratio in the OC NGC



**Table 7.** Comparison of elemental abundance ratios  $[X/Fe]$  for open cluster M 67 using data from various sources.

Species	This study	Tautvaišiene00	Yong05	Pancino10	Friel10
[Na I/Fe]	+0.25 ± 0.02	+0.20 ± 0.00	+0.30 ± 0.05	+0.08 ± 0.09	+0.13 ± 0.06
[Mg I/Fe]	+0.16 ± 0.02	+0.09 ± 0.00	+0.16 ± 0.05	+0.27 ± 0.04	+0.05 ± 0.06
[Al I/Fe]	+0.09 ± 0.01	+0.13 ± 0.02	+0.17 ± 0.03	+0.03 ± 0.02	+0.11 ± 0.04
[Si I/Fe]	+0.20 ± 0.02	+0.09 ± 0.04	+0.09 ± 0.06	+0.10 ± 0.02	+0.18 ± 0.06
[Ca I/Fe]	+0.04 ± 0.02	+0.06 ± 0.10	+0.07 ± 0.02	-0.16 ± 0.03	-0.08 ± 0.08
[Ti I/Fe]	-0.01 ± 0.02	+0.03 ± 0.10	+0.12 ± 0.02	-0.04 ± 0.06	-0.14 ± 0.06
[Cr I/Fe]	+0.05 ± 0.02	+0.07 ± 0.09	...	+0.01 ± 0.03	+0.00 ± 0.02
[Fe I/H]	-0.08 ± 0.02	0.00 ± 0.06	+0.02 ± 0.08	+0.05 ± 0.02	+0.03 ± 0.08
[Ni I/Fe]	+0.10 ± 0.02	+0.06 ± 0.09	+0.08 ± 0.05	+0.05 ± 0.01	-0.02 ± 0.05
[Y II/Fe]	+0.03 ± 0.02	-0.02 ± 0.11	...	-0.05 ± 0.04	...
[Zr I/Fe]	-0.07 ± 0.02	-0.19 ± 0.09	-0.28 ± 0.02	...	-0.14 ± 0.03
[Ba II/Fe]	<b>-0.16 ± 0.06</b>	+0.08 ± 0.00	<b>-0.02 ± 0.05</b>	+0.25 ± 0.02	...
[La II/Fe]	0.00 ± 0.02	+0.12 ± 0.05	+0.11 ± 0.03	+0.05 ± 0.06	...
[Ce II/Fe]	<b>-0.02 ± 0.03</b>	+0.08 ± 0.08	...	...	...
[Nd II/Fe]	+0.02 ± 0.03	...	...	...	...
[Sm II/Fe]	<b>-0.03 ± 0.03</b>	+0.06 ± 0.00	...	...	...
[Eu II/Fe]	<b>+0.08 ± 0.03</b>	<b>+0.07 ± 0.00</b>	<b>+0.06 ± 0.02</b>	...	...

**Note:** Abundances calculated by synthesis are presented in bold numbers and the quoted errors on them are the sensitivity of their abundance to adopted model atmospheric parameters. An internal uncertainty of 0.00 means that the abundance analysis is based on a single line only.

Tautvaišiene00– Tautvaišiene et al. (2000); Yong05– Yong et al. (2005); Pancino10– Pancino et al. (2010); Friel10– Friel et al. (2010);

2266. For these low mass AGB stars, the dominant neutron source is  $^{13}\text{C}(\alpha, n)^{16}\text{O}$  reaction which is responsible for the production of s-process elements to observed values. We note that NGC 2266 has a higher  $[\text{Rb}/\text{Zr}]$  ratio than the other OCs studied here, although our measured Rb abundance is based on a single star. Such a high  $[\text{Rb}/\text{Zr}]$  ratio for the OC NGC 2266, complimented with sub-solar s-process elemental abundances and over-solar r-process and  $\alpha$ -elements, reflects the addition of Type II SNe to the chemical enrichment of its parent gas cloud prior to its formation.

Our present sample includes the well-studied OC NGC 2682 (M 67) for which high-resolution spectroscopic abundance analyses have been reported by Tautvaišiene et al. (2000, hereafter Tautvaišiene00), Yong et al. (2005, hereafter Yong05), Pancino et al. (2010, hereafter Pancino10) and Friel et al. (2010, hereafter Friel10). Unfortunately, none of the above groups, except Tautvaišiene00 sample, have stars in common with our sample for a direct star-to-star comparison of results, but on the assumption that the intrinsic dispersion in abundances within NGC 2682 is negligible, we may compare results from the separate analyses. For the Tautvaišiene00 sample we give in Table 7 the mean of the average abundances of three stars in common with our study and this mean value does not change if we consider the whole sample of stars studied by Tautvaišiene00. Differences in  $[X/Fe]$  between our results and the four published analyses are  $\pm 0.15$  dex or smaller for almost all elements in common: exceptions include Si and Zr for Yong05, Na, Ca, and Ba for Pancino10, Ba for Tautvaišiene00, but all elements considered by Friel10 fall within the  $\pm 0.15$  limit. Further, a direct star-to-star comparison of  $[X/Fe]$  abundance for almost all elements in common between ours and Tautvaišiene00 fall within  $\pm 0.15$  dex with the exception of  $[\text{Ba}/\text{Fe}]$ . The  $[\text{Fe}/\text{H}]$  estimates for the four published analyses are consistent but our result is consistently slightly sub-

solar:  $[\text{Fe}/\text{H}] = -0.08$  versus 0.00 to +0.05. This comparison (Table 7) suggests a quite satisfactory agreement for all elements given the many different choices which enter into a LTE model atmosphere abundance analysis.

It seems very likely that a concerted effort to establish a truly common method of analysis for red giants in OCs for use by all the principal players should minimize or even eliminate systematic abundance differences. Then, a combined set of results for OCs across the Galaxy should reveal novel insights into the development of abundance differences in time and space within the Galactic disc.

## 5 CONCLUSIONS

This study is a part of a project devoted to the measurement of metallicity and chemical abundances of giant stars in OCs covering a broad range of elements, since such measurements are often lacking in the literature, especially for neutron capture elements. We have performed a detailed differential abundance analysis of red giants in seven OCs located in the Galactic anticentre direction at Galactocentric distances of  $R_{gc} \sim 8.3$  to 11.3 kpc. Based on the high resolution spectra and standard LTE analysis, we have derived stellar parameters and abundance ratios for elements from Na to Eu.

The main results of this study are as follows:

(i) We have derived average  $[\text{Fe}/\text{H}]$  values of  $-0.10 \pm 0.04$  for NGC 2527,  $-0.08 \pm 0.04$  for NGC 2682,  $-0.07 \pm 0.04$  for NGC 2482,  $-0.06 \pm 0.04$  for NGC 2539,  $-0.18 \pm 0.03$  for NGC 2335,  $-0.10 \pm 0.05$  for NGC 2251, and  $-0.44 \pm 0.04$  for NGC 2266.

(ii) Our findings confirm the result from Paper 1 that these OC and local disc field giants with  $[\text{Fe}/\text{H}] \sim 0$  have

identical compositions to within the errors of measurements. The observed offset of [Mn/Fe] between the Luck & Heiter's (2007) sample of field giants and the field dwarfs/OC giants might be arising due to the neglect of hfs treatment in their abundance analysis of field giants.

#### Acknowledgments:

We are grateful to the McDonald Observatory's Time Allocation Committee for granting us observing time to this project. DLL wishes to thank the Robert A. Welch Foundation of Houston, Texas for support through grant F-634. We also thank the anonymous referee for useful comments which led to improvements of the paper.

This research has made use of the WEBDA database, operated at the Institute for Astronomy of the University of Vienna and the NASA ADS, USA. This research has also made use of Aladin. This publication makes use of data products from the Two Micron All Sky Survey, which is a joint project of the University of Massachusetts and the Infrared Processing and Analysis Center/California Institute of Technology, funded by the National Aeronautics and Space Administration (NASA) and the National Science Foundation (NSF).

#### REFERENCES

- Allende Prieto C., García López R. J., Lambert D. L., Gustafsson B., 1999, *ApJ*, 527, 879.
- Alonso A., Arribas S., Martínez-Roger C., 1999, *A&AS*, 140, 261
- Asplund M., Grevesse N., Sauval A. J., Scott, P., 2009, *ARA&A*, 47, 481
- Carrera R., 2012, *A&A*, 544, 109
- Carpenter J. M., 2001, *AJ*, 121, 2851
- Castelli F., Kurucz R. L., 2003, *IAU Symposium 210, Modelling of Stellar Atmospheres*, Uppsala, Sweden, eds. N.E. Piskunov, W.W. Weiss, and D.F. Gray, 2003, ASP-S210
- Claria J. J., & Lapasset E., 1986, *ApJ*, 302, 656
- Cutri R.M., Skrutskie M.F., Van Dyk S. et al., 2003, *Vizie Online Data Catalogue*, **II/246**
- Dias W. S., Alessi B. S., Moitinho A., Lépine J. R. D., 2002, *A&A*, 389, 871
- Dinescu D. I., Demarque P., Guenther D. B., & Pinsonneault M. H., 1995, *AJ*, 109, 2090
- De Silva G. M., Sneden C., Paulson D. B., Asplund M., Bland-Hawthorn J., Bessell M. S., Freeman K. C., 2006, *AJ*, 131, 455
- De Silva G. M., Freeman K. C., Bland-Hawthorn J., Asplund M., Bessell M. S., 2007, *AJ*, 133, 694
- Freeman K., Bland-Hawthorn J., 2002, *ARA&A*, 40, 487
- Friel E. D., Jacobson H. R., Pilachowski C. A., 2010, *AJ*, 139, 1942
- Ghez, A. M. et al., 2008, *ApJ*, 689, 1044
- Hinkle K., Wallace L., Valenti J., Harmer D., 2000, *Visible and Near Infrared Atlas of the Arcturus Spectrum 3727-9300 Å* (San Francisco:ASP)
- Kaluzny J., Mazur B., 1991, *AcA*, 41, 191
- Kurucz R. L., Furenlid I., Brault J., & Testerman L. 1984, *Solar Flux Atlas from 296 to 1300 nm*, ed. R. L. Kurucz, I. Furenlid, J. Brault, & L. Testerman (Sunspot, NM: National Solar Observatory)
- Lambert D. L., & Luck R. E., 1976, *Observatory*, 60, 100
- Lawler J. E., Bonvallet G., Sneden C., 2001, *ApJ*, 556, 452
- Luck R. E., Heiter U., 2006, *AJ*, 131, 3069
- Luck R. E., Heiter U., 2007, *AJ*, 133, 2464
- Magrini L., Sestito P., Randich S., Galli D., 2009, *A&A*, 494, 95
- Magrini L., Randich S., Zoccali M., Jilkova L., Carraro G., Galli D., Maiorca E., Busso M., 2010, *A&A*, 523, 11
- Mermilliod J.-C., Mayor M., Udry S., 2008, *A&A*, 485, 303
- Parisi M. C., Claria J. J., Piatti A. E., & Geisler D., 2005, *MNRAS*, 363, 1247
- Pancino E., Carrera R., Rossetti E., Gallart C., 2010, *A&A*, 511, 56
- Piatti A. E., Claria J. J., & Abadi M. G., 1995, *AJ*, 110, 2813
- Reddy B. E., Lambert D. L., Allende Prieto C., 2006, *MNRAS*, 367, 1329
- Reddy A. B. S., Giridhar S., Lambert D. L., 2012, *MNRAS*, 419, 1350 (paper i)
- Smith V. V., Suntzeff N. B., Cunha K., Gallino R., Busso B., Lambert D.L., & Straniero O., 2000, *AJ*, 119, 1239
- Snedden C., 1973, PhD Thesis, Univ. of Texas, Austin
- Takeda Y., 2007, *PASJ*, 59, 335
- Takeda Y., Sato B., Murata D., 2008, *PASJ*, 60, 781
- Tautvaišiene G., Edvardsson B., Tuominen I., Ilyin I., 2000, *A&A*, 360, 499
- Tomkin J., Lambert D. L., 1999, *ApJ*, 523, 324
- Tull R.G., MacQueen P.J., Sneden C., Lambert D.L., 1995, *PASP*, 107, 251
- Twarog B. A., Ashman K. M., & Anthony-Twarog B. J., 1997, *AJ*, 114, 2556
- Wiese W. L., & Martin G. A., 1980, *Wavelengths and Transition Probabilities for Atoms and Atomic Ions*, NSRDS-NBS 68 (Washington, DC: USGPO)
- Yi S.K., Kim Y.-C., Demarque P., 2003, *ApJS*, 144, 259
- Yong D., Carney B. W., Teixeira de Almeida M. L., 2005, *AJ*, 130, 597
- Yong D., Carney B. W., Teixeira de Almeida M. L., Pohl B. L., 2006, *AJ*, 131, 2256

**Table 8.** Elemental abundances for stars in the OC NGC 2527.

Species	star no. 10	star no. 203	Average
[Na I/Fe]	+0.31 ± 0.03(5)	+0.33 ± 0.03(4)	+0.32 ± 0.02
[Mg I/Fe]	+0.07 ± 0.01(4)	+0.08 ± 0.02(5)	+0.07 ± 0.01
[Al I/Fe]	+0.06 ± 0.04(6)	+0.04 ± 0.03(4)	+0.05 ± 0.02
[Si I/Fe]	+0.20 ± 0.03(13)	+0.21 ± 0.03(10)	+0.20 ± 0.02
[Ca I/Fe]	+0.09 ± 0.05(14)	+0.15 ± 0.04(11)	+0.12 ± 0.03
[Sc I/Fe]	+0.30 ± 0.06(6)	+0.21 ± 0.04(7)	+0.25 ± 0.04
[Sc II/Fe]	+0.15 ± 0.05(5)	+0.07 ± 0.04(5)	+0.12 ± 0.03
[Ti I/Fe]	+0.12 ± 0.02(13)	+0.11 ± 0.04(16)	+0.11 ± 0.02
[Ti II/Fe]	+0.08 ± 0.04(6)	+0.09 ± 0.03(7)	+0.08 ± 0.02
[V I/Fe]	+0.24 ± 0.03(14)	+0.18 ± 0.05(16)	+0.21 ± 0.03
[Cr I/Fe]	+0.11 ± 0.04(9)	+0.10 ± 0.04(10)	+0.10 ± 0.03
[Cr II/Fe]	+0.09 ± 0.04(9)	+0.03 ± 0.05(7)	+0.06 ± 0.03
[Mn I/Fe]	<b>-0.03</b>	<b>+0.04</b>	<b>0.00</b>
[Fe I/H]	-0.14 ± 0.04(47)	-0.09 ± 0.04(55)	-0.11 ± 0.03
[Fe II/H]	-0.11 ± 0.04(13)	-0.07 ± 0.03(12)	-0.09 ± 0.02
[Co I/Fe]	+0.21 ± 0.04(4)	+0.11 ± 0.06(4)	+0.16 ± 0.04
[Ni I/Fe]	+0.05 ± 0.04(18)	+0.08 ± 0.03(17)	+0.06 ± 0.02
[Cu I/Fe]	<b>-0.11</b>	<b>-0.18</b>	<b>-0.14</b>
[Zn I/Fe]	<b>-0.17</b>	<b>-0.16</b>	<b>-0.16</b>
[Rb I/Fe]	<b>+0.11</b>	<b>+0.03</b>	<b>+0.07</b>
[Y II/Fe]	+0.17 ± 0.03(5)	+0.15 ± 0.03(5)	+0.16 ± 0.02
[Zr I/Fe]	+0.38 ± 0.07(5)	+0.25 ± 0.07(4)	+0.31 ± 0.05
[Zr II/Fe]	+0.26 ± 0.02(3)	+0.10 ± 0.04(2)	+0.18 ± 0.02
[Ba II/Fe]	<b>+0.09</b>	<b>+0.07</b>	<b>+0.08</b>
[La II/Fe]	+0.26 ± 0.04(3)	+0.27 ± 0.03(3)	+0.26 ± 0.02
[Ce II/Fe]	+0.26	<b>+0.22</b>	<b>+0.24</b>
[Nd II/Fe]	+0.20 ± 0.01(4)	+0.20 ± 0.04(6)	+0.20 ± 0.02
[Sm II/Fe]	<b>+0.19</b>	<b>+0.18</b>	<b>+0.18</b>
[Eu II/Fe]	<b>+0.12</b>	<b>+0.08</b>	<b>+0.10</b>

**Note:** The abundances calculated by synthesis are presented in bold numbers. The remaining elemental abundances were calculated using line equivalent widths. Numbers in the parentheses indicate the number of lines used in calculating the abundance of that element. In this analysis we have adopted the hfs data of Prochaska & McWilliam (2000) for Mn I, Mucciarelli et al. (2008) for Eu II line, McWilliam (1998) for Ba II line, and Allen et al. (2011) for Cu I lines.

**Table 9.** Elemental abundances for stars in the OC NGC 2682.

Species	star no. 84	star no. 151	star no. 164	Average
[Na I/Fe]	+0.23 ± 0.05(6)	+0.27 ± 0.02(6)	+0.26 ± 0.02(6)	+0.25 ± 0.02
[Mg I/Fe]	+0.12 ± 0.04(7)	+0.17 ± 0.04(8)	+0.20 ± 0.04(8)	+0.16 ± 0.02
[Al I/Fe]	+0.09 ± 0.02(5)	+0.05 ± 0.03(4)	+0.12 ± 0.03(6)	+0.09 ± 0.01
[Si I/Fe]	+0.19 ± 0.04(13)	+0.18 ± 0.05(14)	+0.23 ± 0.03(15)	+0.20 ± 0.02
[Ca I/Fe]	+0.06 ± 0.03(14)	+0.02 ± 0.05(13)	+0.03 ± 0.03(15)	+0.04 ± 0.02
[Sc I/Fe]	+0.11 ± 0.04(4)	+0.01 ± 0.05(6)	-0.01 ± 0.06(7)	+0.04 ± 0.03
[Sc II/Fe]	+0.20 ± 0.01(4)	+0.09 ± 0.06(3)	0.00 ± 0.04(2)	+0.10 ± 0.02
[Ti I/Fe]	+0.06 ± 0.04(18)	-0.04 ± 0.04(19)	-0.06 ± 0.04(18)	-0.01 ± 0.02
[Ti II/Fe]	+0.08 ± 0.02(9)	-0.01 ± 0.04(9)	-0.03 ± 0.02(7)	+0.01 ± 0.02
[V I/Fe]	+0.13 ± 0.05(13)	+0.08 ± 0.04(12)	+0.06 ± 0.04(14)	+0.09 ± 0.02
[Cr I/Fe]	+0.08 ± 0.03(14)	+0.02 ± 0.04(18)	+0.05 ± 0.03(14)	+0.05 ± 0.02
[Cr II/Fe]	+0.09 ± 0.02(9)	+0.06 ± 0.05(10)	+0.10 ± 0.02(10)	+0.08 ± 0.02
[Mn I/Fe]	<b>-0.08</b>	<b>-0.12</b>	<b>-0.03</b>	<b>-0.08</b>
[Fe I/H]	-0.08 ± 0.03(66)	-0.06 ± 0.04(64)	-0.11 ± 0.04(64)	-0.08 ± 0.02
[Fe II/H]	-0.07 ± 0.04(11)	-0.06 ± 0.04(10)	-0.11 ± 0.03(11)	-0.08 ± 0.02
[Co I/Fe]	+0.14 ± 0.04(4)	+0.06 ± 0.05(4)	+0.13 ± 0.02(5)	+0.11 ± 0.02
[Ni I/Fe]	+0.11 ± 0.03(20)	+0.08 ± 0.03(21)	+0.10 ± 0.04(20)	+0.10 ± 0.02
[Cu I/Fe]	<b>+0.05</b>	<b>+0.01</b>	<b>-0.16</b>	<b>-0.03</b>
[Zn I/Fe]	<b>+0.04</b>	<b>-0.12</b>	<b>-0.14</b>	<b>-0.07</b>
[Rb I/Fe]	<b>-0.10</b>	<b>-0.19</b>	<b>-0.11</b>	<b>-0.10</b>
[Y II/Fe]	+0.07 ± 0.04(5)	-0.01 ± 0.02(6)	+0.04 ± 0.02(7)	+0.03 ± 0.02
[Zr I/Fe]	0.00 ± 0.04(7)	-0.11 ± 0.03(7)	-0.11 ± 0.05(7)	-0.07 ± 0.02
[Zr II/Fe]	-0.01 ± 0.03(2)	-0.07 ± 0.05(3)	-0.13 ± 0.00(1)	-0.07 ± 0.03
[Ba II/Fe]	<b>-0.16</b>	<b>-0.16</b>	<b>-0.17</b>	<b>-0.16</b>
[La II/Fe]	+0.09 ± 0.03(6)	-0.03 ± 0.04(6)	-0.07 ± 0.02(6)	0.00 ± 0.02
[Ce II/Fe]	<b>-0.09</b>	<b>+0.01</b>	<b>+0.02</b>	<b>-0.02</b>
[Nd II/Fe]	+0.07 ± 0.07(7)	-0.02 ± 0.03(10)	0.00 ± 0.03(10)	+0.02 ± 0.03
[Sm II/Fe]	<b>+0.02</b>	<b>-0.07</b>	<b>-0.04</b>	<b>-0.03</b>
[Eu II/Fe]	<b>+0.12</b>	<b>+0.07</b>	<b>+0.05</b>	<b>+0.08</b>

**Note:** Same as in table 8.

**Table 10.** Elemental abundances for stars in the OC NGC 2539.

Species	star no. 346	star no. 463	Average
[Na I/Fe]	+0.27 ± 0.01(4)	+0.27 ± 0.04(4)	+0.27 ± 0.02
[Mg I/Fe]	+0.06 ± 0.05(5)	+0.08 ± 0.02(4)	+0.07 ± 0.02
[Al I/Fe]	-0.05 ± 0.02(5)	+0.05 ± 0.01(4)	0.00 ± 0.01
[Si I/Fe]	+0.14 ± 0.03(12)	+0.21 ± 0.03(12)	+0.17 ± 0.02
[Ca I/Fe]	+0.02 ± 0.04(12)	+0.06 ± 0.04(15)	+0.04 ± 0.03
[Sc I/Fe]	+0.21 ± 0.03(7)	+0.21 ± 0.04(5)	+0.21 ± 0.02
[Sc II/Fe]	+0.05 ± 0.06(5)	+0.03 ± 0.05(5)	+0.04 ± 0.04
[Ti I/Fe]	+0.10 ± 0.04(15)	+0.11 ± 0.04(14)	+0.10 ± 0.03
[Ti II/Fe]	+0.08 ± 0.03(7)	+0.08 ± 0.05(6)	+0.08 ± 0.03
[V I/Fe]	+0.18 ± 0.05(13)	+0.14 ± 0.04(13)	+0.16 ± 0.03
[Cr I/Fe]	+0.10 ± 0.03(10)	+0.07 ± 0.04(8)	+0.08 ± 0.02
[Cr II/Fe]	+0.09 ± 0.02(6)	+0.07 ± 0.03(6)	+0.08 ± 0.02
[Mn I/Fe]	<b>0.00</b>	<b>+0.02</b>	<b>+0.01</b>
[Fe I/H]	-0.07 ± 0.04(51)	-0.05 ± 0.04(66)	-0.06 ± 0.03
[Fe II/H]	-0.07 ± 0.03(13)	-0.07 ± 0.04(14)	-0.07 ± 0.02
[Co I/Fe]	+0.13 ± 0.04(4)	+0.01 ± 0.04(6)	+0.07 ± 0.03
[Ni I/Fe]	0.00 ± 0.04(17)	+0.05 ± 0.03(21)	+0.02 ± 0.02
[Cu I/Fe]	<b>-0.18</b>	<b>-0.15</b>	<b>-0.16</b>
[Zn I/Fe]	<b>-0.23</b>	<b>-0.22</b>	<b>-0.22</b>
[Rb I/Fe]	<b>+0.07</b>	<b>+0.01</b>	<b>+0.04</b>
[Y II/Fe]	+0.15 ± 0.05(6)	+0.19 ± 0.04(5)	+0.17 ± 0.03
[Zr I/Fe]	+0.23 ± 0.07(5)	+0.19 ± 0.03(5)	+0.21 ± 0.04
[Zr II/Fe]	+0.28 ± 0.04(2)	+0.25 ± 0.03(2)	+0.26 ± 0.02
[Ba II/Fe]	<b>+0.13</b>	<b>+0.08</b>	<b>+0.10</b>
[La II/Fe]	+0.18 ± 0.02(4)	+0.18 ± 0.04(5)	+0.18 ± 0.02
[Ce II/Fe]	<b>+0.21</b>	<b>+0.20</b>	<b>+0.20</b>
[Nd II/Fe]	+0.22 ± 0.05(5)	+0.24 ± 0.03(5)	+0.23 ± 0.03
[Sm II/Fe]	<b>+0.16</b>	<b>+0.20</b>	<b>+0.18</b>
[Eu II/Fe]	<b>+0.19</b>	<b>+0.19</b>	<b>+0.19</b>

**Note:** Same as in table 8.

**Table 11.** Elemental abundances for stars in the OC NGC 2251.

Species	star no. 3	star no. 33	Average
[Na I/Fe]	+0.36 ± 0.04(4)	+0.31 ± 0.04(4)	+0.33 ± 0.03
[Mg I/Fe]	+0.10 ± 0.05(6)	+0.02 ± 0.05(5)	+0.06 ± 0.03
[Al I/Fe]	+0.03 ± 0.04(5)	-0.02 ± 0.03(5)	0.00 ± 0.02
[Si I/Fe]	+0.21 ± 0.01(14)	+0.25 ± 0.05(14)	+0.23 ± 0.02
[Ca I/Fe]	+0.10 ± 0.04(16)	+0.08 ± 0.03(13)	+0.09 ± 0.02
[Sc I/Fe]	+0.09 ± 0.03(5)	-0.01 ± 0.03(3)	+0.04 ± 0.02
[Sc II/Fe]	<b>+0.01</b>	<b>+0.03</b>	<b>+0.02</b>
[Ti I/Fe]	-0.01 ± 0.04(18)	-0.07 ± 0.04(15)	-0.04 ± 0.03
[Ti II/Fe]	-0.06 ± 0.04(8)	-0.02 ± 0.05(4)	-0.04 ± 0.03
[V I/Fe]	-0.01 ± 0.04(16)	-0.10 ± 0.03(13)	-0.05 ± 0.02
[Cr I/Fe]	+0.08 ± 0.05(10)	+0.02 ± 0.05(8)	+0.05 ± 0.03
[Cr II/Fe]	0.00 ± 0.05(8)	+0.08 ± 0.05(7)	+0.04 ± 0.03
[Mn I/Fe]	<b>-0.12</b>	<b>-0.14</b>	<b>-0.13</b>
[Fe I/H]	-0.11 ± 0.04(56)	-0.09 ± 0.05(57)	-0.10 ± 0.03
[Fe II/H]	-0.11 ± 0.04(11)	-0.09 ± 0.04(12)	-0.10 ± 0.03
[Co I/Fe]	+0.08 ± 0.05(6)	-0.01 ± 0.04(5)	+0.03 ± 0.03
[Ni I/Fe]	+0.05 ± 0.04(22)	+0.04 ± 0.04(17)	+0.04 ± 0.03
[Cu I/Fe]	<b>-0.19</b>	<b>-0.27</b>	<b>-0.22</b>
[Zn I/Fe]	<b>-0.11</b>	<b>-0.16</b>	<b>-0.13</b>
[Rb I/Fe]	<b>-0.17</b>	<b>-0.18</b>	<b>-0.17</b>
[Y II/Fe]	+0.05 ± 0.03(5)	+0.10 ± 0.05(5)	+0.07 ± 0.03
[Zr I/Fe]	+0.03 ± 0.05(5)	-0.02 ± 0.03(4)	0.00 ± 0.03
[Zr II/Fe]	+0.06 ± 0.01(2)	+0.06 ± 0.02(2)	+0.06 ± 0.01
[Ba II/Fe]	<b>+0.12</b>	<b>+0.10</b>	<b>+0.11</b>
[La II/Fe]	+0.05 ± 0.04(5)	0.00 ± 0.03(3)	+0.02 ± 0.02
[Ce II/Fe]	<b>+0.07</b>	<b>+0.08</b>	<b>+0.07</b>
[Nd II/Fe]	+0.08 ± 0.03(9)	+0.09 ± 0.04(8)	+0.08 ± 0.02
[Sm II/Fe]	<b>+0.03</b>	<b>+0.01</b>	<b>+0.02</b>
[Eu II/Fe]	<b>+0.05</b>	<b>+0.04</b>	<b>+0.04</b>

**Note:** Same as in table 8.



**Table 12.** Elemental abundances for stars in the OCs NGC 2482, NGC 2335 and NGC 2266.

Species	star no. 2482#9	star no. 2335#11	star no. 2266#73
[Na I/Fe]	+0.30 ± 0.03(6)	+0.24 ± 0.02(6)	+0.23 ± 0.03(5)
[Mg I/Fe]	+0.13 ± 0.02(4)	+0.08 ± 0.02(6)	+0.39 ± 0.02(5)
[Al I/Fe]	+0.07 ± 0.02(4)	-0.02 ± 0.02(6)	+0.25 ± 0.02(5)
[Si I/Fe]	+0.23 ± 0.04(13)	+0.10 ± 0.02(15)	+0.28 ± 0.02(15)
[Ca I/Fe]	+0.01 ± 0.05(15)	+0.09 ± 0.04(15)	+0.17 ± 0.05(16)
[Sc I/Fe]	+0.12 ± 0.05(6)	+0.13 ± 0.04(3)	+0.31 ± 0.05(3)
[Sc II/Fe]	+0.08 ± 0.05(4)	<b>+0.16</b>	+0.22 ± 0.05(5)
[Ti I/Fe]	+0.01 ± 0.04(14)	+0.17 ± 0.04(14)	+0.23 ± 0.04(16)
[Ti II/Fe]	-0.03 ± 0.04(7)	+0.12 ± 0.04(10)	+0.30 ± 0.04(7)
[V I/Fe]	+0.10 ± 0.05(16)	+0.13 ± 0.04(10)	+0.20 ± 0.06(17)
[Cr I/Fe]	+0.10 ± 0.04(12)	+0.07 ± 0.03(10)	+0.09 ± 0.03(12)
[Cr II/Fe]	+0.09 ± 0.05(7)	0.00 ± 0.04(8)	+0.02 ± 0.04(9)
[Mn I/Fe]	<b>-0.11</b>	<b>-0.01</b>	<b>-0.01</b>
[Fe I/H]	-0.07 ± 0.04(62)	-0.19±0.04(59)	-0.45±0.04(88)
[Fe II/H]	-0.07 ± 0.05(12)	-0.17±0.03(12)	-0.43±0.05(12)
[Co I/Fe]	+0.11 ± 0.03(7)	+0.16±0.03(3)	+0.27 ± 0.03(5)
[Ni I/Fe]	+0.03 ± 0.04(17)	+0.09±0.03(21)	+0.09 ± 0.03(20)
[Cu I/Fe]	<b>-0.21</b>	<b>-0.15</b>	<b>+0.02</b>
[Zn I/Fe]	<b>-0.22</b>	<b>-0.06</b>	<b>0.00</b>
[Rb I/Fe]	<b>-0.13</b>	<b>+0.08</b>	<b>+0.14</b>
[Y II/Fe]	+0.15 ± 0.04(5)	+0.12±0.05(5)	+0.05 ± 0.04(4)
[Zr I/Fe]	+0.11 ± 0.05(5)	+0.06±0.04(2)	-0.08±0.05(5)
[Zr II/Fe]	+0.10 ± 0.04(3)	+0.01 ± 0.02(2)	...
[Ba II/Fe]	<b>+0.09</b>	<b>+0.25</b>	<b>-0.13</b>
[La II/Fe]	+0.18 ± 0.03(5)	+0.29±0.03(4)	-0.02 ± 0.04(6)
[Ce II/Fe]	<b>+0.11</b>	<b>+0.29</b>	<b>-0.07</b>
[Nd II/Fe]	+0.13 ± 0.04(7)	+0.32±0.03(8)	+0.13 ± 0.04(4)
[Sm II/Fe]	+0.13 ± 0.04(4)	+0.28±0.03(3)	<b>+0.11</b>
[Eu II/Fe]	<b>+0.07</b>	<b>+0.07</b>	<b>+0.40</b>

**Note:** Same as in table 8.